FRONTIERS OF PHYSICS

RESEARCH ARTICLE
Volume 19 / Issue 3 / 33201 / 2024

Intrinsically asymmetric atomic character regulates piezoelectricity in two-dimensional materials

Yun-Qin Li[1,2], Qi-Wen He[3], Dai-Song Tang[3], Xiao Shang[3], Xiao-Chun Wang[1,3,†]

1 School of Physics Science and Information Technology, Liaocheng University, Liaocheng 252000, China
2 Key Laboratory of Polar Materials and Devices, Ministry of Education, Department of Electronics, East China Normal University, Shanghai 200241, China
3 Institute of Atomic and Molecular Physics, Jilin University, Changchun 130012, China
Corresponding author. E-mail: †wangxiaochun@tsinghua.org.cn
Received August 9, 2023; accepted September 12, 2023

ABSTRACT

Decreasing of layer thickness causes the decrease of polarization until it disappears due to the existence of depolarization field. Therefore, the search for strong piezoelectric materials is highly desirable for multifunctional ultra-thin piezoelectric devices. Herein, we propose a common strategy for achieving strong piezoelectric materials through the electronic asymmetry induced by the intrinsically asymmetric atomic character of different chalcogen atoms. Accordingly, in the tetrahedral lattice structures, for example, $M_4X_3Y_3$ (M = Pd/Ni, X/Y = S, Se or Te, X ≠ Y) monolayers are proved to display excellent out-of-plane piezoelectricity. $Ni_4Se_3Te_3$ possesses the largest piezoelectric coefficient d_{33} of 61.57 pm/V, which is much larger than that of most 2D materials. Enhancing the electronic asymmetry further increases the out-of-plane piezoelectricity of Janus $M_4X_3Y_3$ materials. Correspondingly, the out-of-plane piezoelectricity is positively correlated with the ratio of electronegativity difference (R_{ed}) and the electric dipole moment (P). This work provides alternative materials for energy harvesting nano-devices or self-energized wearable devices, and supplies a valuable guideline for predicting 2D materials with strong out-of-plane piezoelectricity.

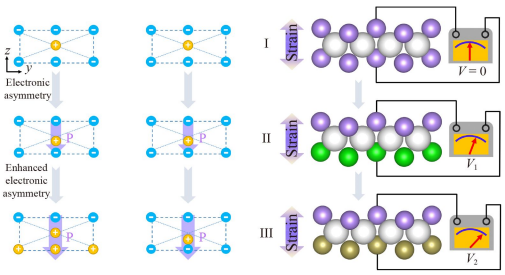

Keywords piezoelectricity, intrinsically asymmetric atomic character, ratio of electronegativity difference, electric dipole moment, first-principles calculations

1 Introduction

Two-dimensional (2D) graphene has been successfully exfoliated experimentally [1], and it has been found that 2D graphene has good physicochemical properties such as ultra-high carrier mobility and the fermi Dirac point. Graphene doped with metal atoms can be used as a catalyst to achieve photocatalytic hydrolysis [2, 3]. In addition to graphene, other 2D materials have received a lot of attention [4–6], such as the transition metal sulfides (TMDCs) [7–11], MXenes [12], MBenes [13, 14], and sandwich-like $MoSi_2N_4$ monolayer [15–17]. Piezoelectric materials can realize the mutual conversion between mechanical energy and electric energy, which are widely used in the design of sensors, and microelectromechanical devices. For example, piezoelectric materials can be used to design flexible electronics, flexible screens, health monitoring devices, and electronic sensing skin [18].

Higher Education Press

https://doi.org/10.1007/s11467-023-1348-5

Recent years, piezoelectric materials have also been applied to some blue energy harvesting, such as the wind, water power, waves and other large signal energy harvesting [19]. In addition, piezoelectric devices are also applied to the conversion of tiny mechanical energies that are often neglected, such as walking, body shaking and hand touching [20, 21]. Therefore, to achieve the collection of tiny mechanical energy, it is important to find piezoelectric materials with good stability, strong mechanical durability and strong piezoelectric response.

Materials with the out-of-plane piezoelectric properties can produce piezoelectric response to the vertical strain in the out-of-plane direction, converting mechanical stress perpendicular to the monolayer plane into electrical energy [22, 23]. Cutting-edge piezoelectric equipment such as the wearable electronics, medical blood pressure detectors and robotic bionic skin tactile sensors really utilize the out-of-plane piezoelectricity. Therefore, we make unremitting efforts to find excellent and intriguing stable 2D materials with remarkable out-of-plane piezoelectricity. Previous studies show that the transition metal dichalcogenides (TMDCs) with the in-plane piezoelectric properties can produce piezoelectric responses to internal strains, but not to vertical strains [24–28]. The symmetry of TMDCs-like materials with low symmetry C_{3v} space group is broken along the z axis direction, which makes them contain the out-of-plane piezoelectricity, such as the VSSe [29], MoSSe [30] or MoTO (T = S, Se, or Te) [31].

Previous studies have reported that Pd_2Se_3 films can be successfully fabricated experimentally, and it has interesting physicochemical properties, such as medium-sized band gap and high carrier mobility [32–34]. In addition, the Co_2Se_3 monolayer with semi-metallic properties and ultra-high mechanical stability can be obtained by substituting Pd atoms with Co atoms [35, 36]. These Pd_2Se_3 and Co_2Se_3 monolayers have similar side view to that of TMDCs monolayers with 2H phase. That is, the transition metal atoms are located in the intermediate layer, surrounded by chalcogenide Se atoms. Based on the $PdSe_2$, the Pd_2Se_3 was successfully fabricated in experiments using electron beam irradiation [34]. Recently, $Pd_4S_3Se_3$, $Pd_4S_3Te_3$, and $Pd_4Se_3Te_3$ monolayers have been proved to be excellent photocatalyst candidates with suitable bandgaps for photocatalytic water splitting [37]. However, as far as we know, the piezoelectricity of these Janus two-dimensional materials has not been studied.

In this work, therefore, we propose a common scheme to obtain strong piezoelectric materials, where different chalcogen atoms with intrinsically asymmetric atomic character can induce the electronic asymmetry. The piezoelectricity of the $M_4X_3Y_3$ (M = Pd/Ni, X/Y = S, Se or Te, X ≠ Y) Janus materials is theoretically predicted for the first time. Mirror electronic asymmetry leads to the introduction of the strong out-of-plane piezoelectricity. Enhancing the electronic asymmetry further increases the out-of-plane piezoelectricity. Accordingly, piezoelectric coefficients of $Pd_4X_3Y_3$ are positively related with the electronegative difference ratio R_{ed} and the electric diploe moment P, which opens a way for designing strong out-of-plane piezoelectric materials.

2 Computational details

First-principles calculations in this study are performed by Vienna *ab initio* Simulation Package (VASP) with the projected augmented wave (PAW) [38 39]. The Perdew-Burke-Ernzerhof (PBE) exchange-correlation functional within generalized gradient approximations (GGA) is carried out for the structural fully optimizations of $M_4X_3Y_3$ monolayers [40]. The energy and atomic force convergence criteria are set to 10^{-7} eV and 0.0001 eV/Å, respectively. The energy cutoff is set to 550 eV, which is accurate enough to describe the outer valence electrons of Pd, Ni, S, Se and Te atoms. A higher than 20 Å of thick vacuum slab is considered to avoid neighboring-layers interaction. After a test of k-points [in Fig. S1 of the Electronic Supplementary Materials (ESM)], the Γ-centered 9 × 9 × 1 Monkhorst–Pack k-point meshs is used to sample the first Brillouin zone. Phonon spectra used to judge the dynamic stability are performed by the finite difference method [41]. Thermal stability is estimated by the *ab initio* molecular dynamics (AIMD) simulations [42]. In order to obtain the accurate band electronic structures for $M_4X_3Y_3$ monolayers, the Heyd–Scuseria–Ernzerhof (HSE06) hybrid functional [43] are performed. The Bader charge analysis technique [44] is used to analyze the uneven charge distributions. Using the small displacement methodology [45] to calculate the elastic stiffness tensors C_{kj}.

3 Results and discussion

Polarization usually originates from the non-overlapping of opposite charge centers, which occurs in crystals with low-symmetry space groups. Using the intrinsically asymmetric atomic character of different chalcogen atom is a method of inducing the electronic asymmetry in tetrahedral lattices (Fig. 1), and then introducing polarization. Furthermore, the polarization intensity can be further increased by enhancing electronic asymmetry. In Pd_2X_3 and Ni_2X_3 (X = S, Se or Te) monolayers [Figs. 1(a) and (b)], Pd atoms are positively charged by losing charges, so the positive charge center is located at the diagonal center of the rectangular lattice. While the top and bottom negatively charged X atoms are located along the x- and y-axis of the rectangular lattice. Therefore, the positive charge center is coincided with the negative charge center, and the in-plane and out-of-

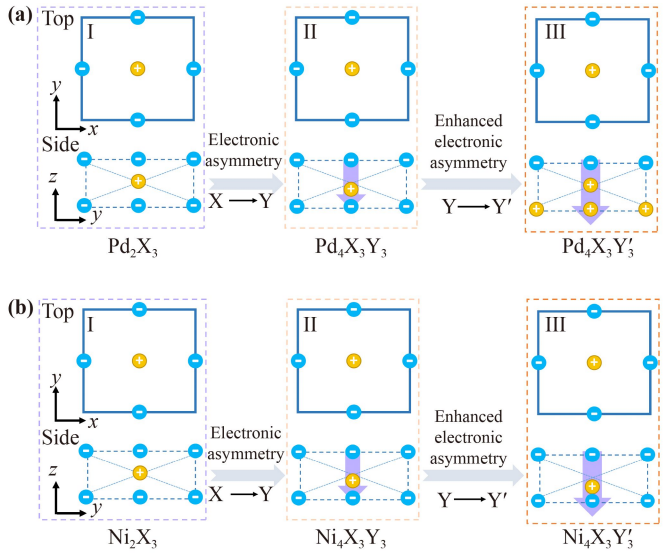

Fig. 1 Schematic diagram of induced out-of-plane polarization in the 2D rectangular structure lattice (from phase I to III). The purple arrow indicates the polarization vector point toward the $-z$ axis direction.

plane piezoelectric effect are missing in the Pd_2X_3 and Ni_2X_3 structures. However, this balance is broken by replacing different chalcogen atoms with intrinsically asymmetric atomic character (from phase I to II). In other words, replacing one side X atoms with Y atoms to obtain the $Pd_4X_3Y_3$ and $Ni_4X_3Y_3$ with piezoelectricity. Finally, further enhance the piezoelectricity by strengthening electronic asymmetry (from phase II to III). In twisted rectangular lattice $Pd_4X_3Y'_3$ monolayer, increasing the difference between the top and bottom chalcogen atoms will cause the bottom chalcogen atoms to lose electrons and show positive charge, therefore strengthen the out-of-plane piezoelectricity. While in $Ni_4X_3Y'_3$ monolayer, the bottom layer atoms still being negatively charged when further increasing the difference between X and Y′ atoms. However, this behavior increases the dipole moment between the positive and negative charge centers, thus can strengthen the piezoelectricity of $Ni_4X_3Y'_3$. In addition to rectangular lattice structure, other 2D structures (such as the TMDs with the 1T phase [46]) can also introduce high vertical polarization by following the same strategy.

Top and side views of the fully optimized $M_4X_3Y_3$ (M = Pd/Ni, X/Y = S, Se or Te, X ≠ Y) monolayers with a X–X–M–Y–Y five-layer atomic structure as shown in Fig. 2(a). These $Pd_4X_3Y_3$ and $Ni_4X_3Y_3$ monolayers can be constructed by replacing the chalcogen atoms on one side of the Pd_2X_3 and Ni_2X_3 (X = S, Se or Te) structures [34, 47–49] with different chalcogen atoms. Different from the Pd_2X_3 and Ni_2X_3 monolayers, $Pd_4X_3Y_3$ and $Ni_4X_3Y_3$ monolayers with mirror symmetry breaking contain the space group *Pmm*2 (No. 25). A unit cell of a $M_4X_3Y_3$ monolayer consists of four M metal atoms, three chalcogen X atoms and Y chalcogen atoms, forming a rectangular structure. In the unit cell of a $M_4X_3Y_3$ monolayer, six different types of bonds can be found. As shown in Fig. 2(b), four 2X–M–2Y pentatomic planes form a $M_4X_3Y_3$ structure. The lattice parameters a and b (in Table S1) for the fully-relaxed $Pd_4S_3Se_3$, $Pd_4S_3Te_3$, $Pd_4Se_3Te_3$, $Ni_4S_3Se_3$, $Ni_4S_3Te_3$ and $Ni_4Se_3Te_3$ monolayers are 5.87 Å and 6.03 Å, 5.92 Å and 6.27 Å, 6.05 Å and 6.39 Å, 5.32 Å and 5.76 Å, 5.35 Å and 6.20 Å, 5.46 Å and 6.38 Å, respectively. Layer thickness h of $Pd_4S_3Se_3$, $Pd_4S_3Te_3$, $Pd_4Se_3Te_3$, $Ni_4S_3Se_3$, $Ni_4S_3Te_3$ and $Ni_4Se_3Te_3$ monolayers are 3.73 Å, 3.94 Å, 4.05 Å, 3.58 Å, 3.79 Å and 3.91 Å, respectively. These results are completely consistent with that of previous reports [37, 48]. As is well known that a large electron localization function (ELF) value (> 0.5) corresponds to a covalent bond, whereas the ionic bond is represented by a smaller ELF value (< 0.5). An ELF value of 0.5 represents the metallic bond. Herein, according to analysis of the ELF diagrams

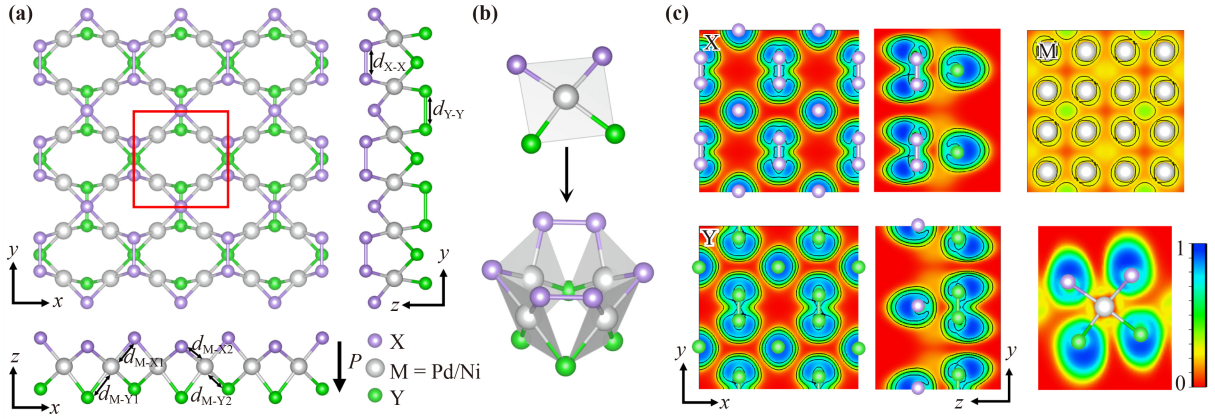

Fig. 2 **(a)** Top and side views of the $M_4X_3Y_3$ monolayers. **(b)** Four 2X–M–2Y pentatomic planes form a $M_4X_3Y_3$ structure. **(c)** Electron localization function (ELF) map of the top X, middle M, bottom Y layers, and the ELF map of the 2X–M–2Y pentatomic planes.

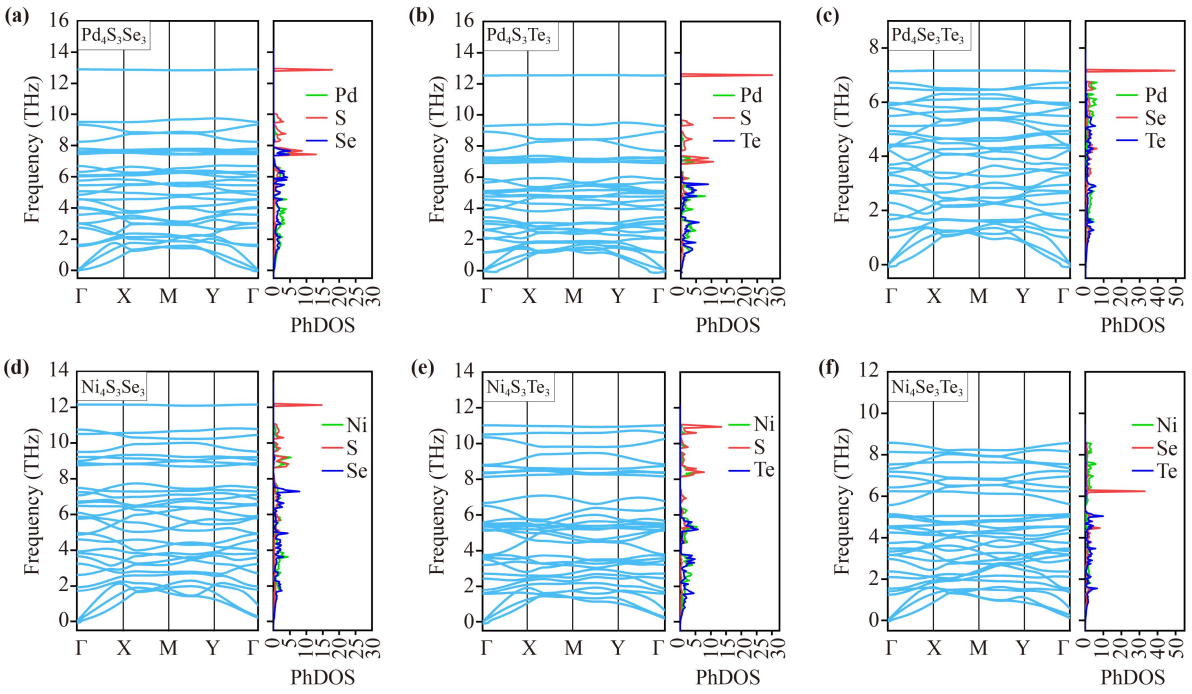

Fig. 3 **(a–f)** The Phonon spectra with the projected phonon density of states (PhDOS) for $M_4X_3Y_3$ monolayers.

[Fig. 2(c)], two adjacent X (Y) atoms on the upper X and lower Y planes along the y lattice form the covalent bonds in a $M_4X_3Y_3$ monolayer. According to the ELF map of the 2X–M–2Y pentatomic planes, each M atom form two ionic bonds with two X and Y atoms, respectively. Values of $d_{M\text{-}X1}$, $d_{M\text{-}X2}$, $d_{M\text{-}Y1}$, $d_{M\text{-}Y2}$, $d_{X\text{-}X}$ and $d_{Y\text{-}Y}$ (in Table S1 of the ESM) have the same order trend in $M_4X_3Y_3$ monolayers, i.e., $Pd_4S_3Se_3$ < $Pd_4S_3Te_3$ < $Pd_4Se_3Te_3$, $Ni_4S_3Se_3$ < $Ni_4S_3Te_3$ < $Ni_4Se_3Te_3$. Due to the different electronegativity of X and Y atoms, these monolayers contain the asymmetric structure, which is critical for the introduction of vertical polarization P pointing to the $-z$ direction [Fig. 2(a), the black arrow].

$M_4X_3Y_3$ monolayers contain great dynamic stabilities demonstrated by the phonon spectra with no appreciable imaginary frequency in the first Brillouin zone (Fig. 3). Except the $Ni_4Se_3Te_3$, the maximum frequencies in the phonon spectrum are contributed by the atoms with the largest electronegativity. For example, the maximum frequency of $Pd_4S_3Se_3$ is contributed by S atoms with largest electronegativity of 2.58, showing the mechanical robustness of the covalent S–S bonds. In addition, they also exhibit great thermal stability properties in ambient temperature [48] and high temperature, verifying by the results of the AIMD simulations (Fig. S2 of the ESM). From Fig. S3 of the ESM, the spin-orbit coupling (SOC) has little influence on the electronic properties for these $M_4X_3Y_3$ monolayers, and their non-magnetic state can be maintained. The bandgaps for $M_4X_3Y_3$ monolayer reduce a little, and the maximum shifting value is about 0.02 eV, accounting for 8%. Results of electronic band structures at HSE level (Fig. S4 of the ESM) suggest they are indirect semiconductors with band gaps of 1.46 eV ($Pd_4S_3Se_3$), 0.54 eV ($Pd_4S_3Te_3$) and 1.41 eV ($Pd_4Se_3Te_3$), 1.65 eV ($Ni_4S_3Se_3$), 0.66 eV ($Ni_4S_3Te_3$) and 0.79 eV ($Ni_4Se_3Te_3$), which is consistent with previous study [48]. Accordingly, the semiconductor characteristics and flexible mechanical properties are beneficial to the spontaneous introduction of excellent piezoelectricity in $M_4X_3Y_3$ monolayers.

Piezoelectricity is closely related with the charge distributions. The electronegativities of Pd, Ni, S, Se, and Te atoms are 2.20, 1.91, 2.58, 2.55, and 2.10, respectively, leading the uneven charge distributions in $M_4X_3Y_3$ monolayers. Therefore, as shown in Fig. S5 of the ESM, the vacuum energy levels of the top and bottom surfaces in $M_4X_3Y_3$ monolayers are unequal, with the discontinuities $\Delta\Phi$ of 0.58 eV (for $Pd_4S_3Se_3$), 1.20 eV (for $Pd_4S_3Te_3$) and 0.63 eV (for $Pd_4Se_3Te_3$), 0.62 eV (for $Ni_4S_3Se_3$), 1.27 eV (for $Ni_4S_3Te_3$) and 0.66 eV (for $Ni_4Se_3Te_3$), which are larger than that of some previous studies [50–52]. The vacuum energy levels discontinuities $\Delta\Phi$ allow $M_4X_3Y_3$ monolayers to generate a vertical built-in electric field, favoring the introduction of the out-of-plane polarization. Uneven charge distribution in the $M_4X_3Y_3$ monolayers can also be confirmed by the planar-average charge density (Fig. 4) along the z direction. The charge density difference is calculated by [53, 54]: $\Delta\rho(\boldsymbol{r}) = \rho(M_4X_3Y_3) - \sum_\mu \rho_{atom}(\boldsymbol{r} - \boldsymbol{R}_\mu)$, where the $\rho(M_4X_3Y_3)$ is the charged density of $M_4X_3Y_3$ monolayers, and $\sum_\mu \rho_{atom}(\boldsymbol{r} - \boldsymbol{R}_\mu)$ is the superposition of charge densities of each atom. Taking the $Pd_4S_3Se_3$ monolayer

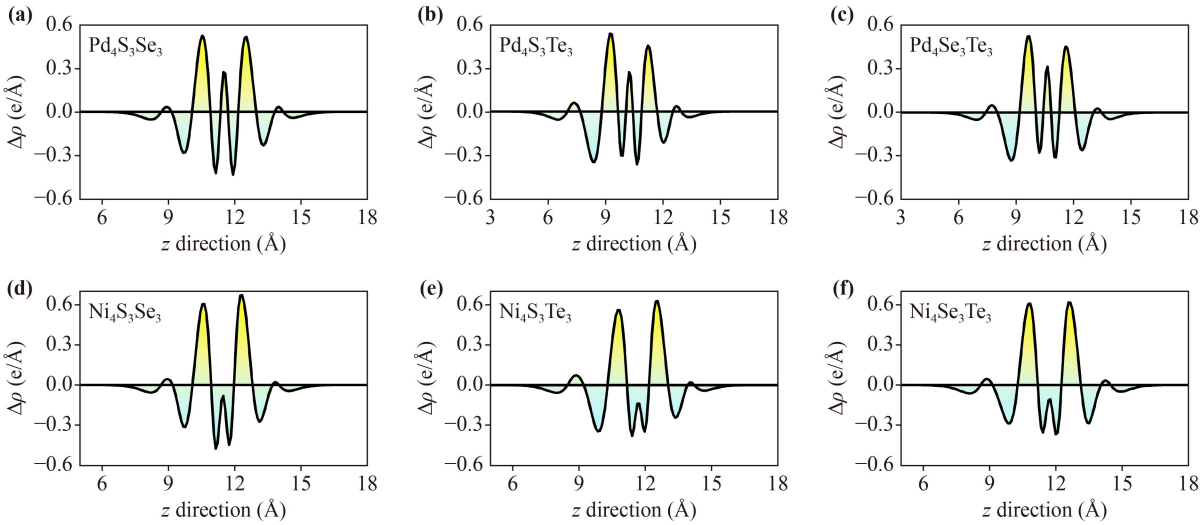

Fig. 4 **(a–f)** planar-average charge density along the z direction for the $M_4X_3Y_3$ monolayers. Yellow and blue regions refer to the electron accumulation and depletion with 0.006 e/bohr^3 isosurfaces.

as example, each Pd atoms with smallest electronegativity lose electrons of 0.237 |e| and are positively charged, while S and Se atoms gain electrons and are negatively charged. Interestingly, in $Pd_4S_3Te_3$ and $Pd_4Se_3Te_3$ monolayers, the Te atoms with the smallest electronegativity lose electrons and are positively charged, while the S, Se and Pd atoms gain electrons and negatively charged.

We found that the five $M_4X_3Y_3$ monolayers possess great mechanical stability, C_{kl} (in Table S2) meet the meet the Born-Huang mechanical stability rules [55]: $(C_{11}C_{22}–C_{12}C_{12}) > 0$ and $C_{66} > 0$). However, the $Ni_4S_3Te_3$ monolayer does not have the mechanical stability, so we then focus on the piezoelectric properties of other five $M_4X_3Y_3$ monolayers. From Fig. S6 of the ESM, $M_4X_3Y_3$ monolayers exhibit anisotropic elastic properties verified by the anisotropic Young's modulus $Y(\theta)$ and Poisson's ratio $v(\theta)$. Compared with previous reported 2D monolayers, such as the graphene [55] and MoX_2 (X = S, Se or Te) [7], $M_4X_3Y_3$ monolayers contain smaller $Y(\theta)$ and larger $v(\theta)$, demonstrating that $M_4X_3Y_3$ are soft and possess great flexibility. These flexible mechanical properties contribute to the spontaneous piezoelectricity of $M_4X_3Y_3$ monolayers. Especially, $Ni_4Se_3Te_3$ possess the smallest $Y(\theta)$ and largest $v(\theta)$, reflecting its strongest flexibility and strongest piezoelectric response. The piezoelectric stress and strain coefficients for $M_4X_3Y_3$ monolayers are calculated to have a visual insight into their out-of-plane piezoelectricity. The coupling between the electrical polarization P_i and the stress ε_{jk} and stain σ_{jk} tensor can be described by the third-rank tensor $e_{ijk} = \partial P_i/\partial\varepsilon_{jk}$ and $d_{ijk} = \partial P_i/\partial\sigma_{jk}$, i, j and k represent the x, y and z directions. By using the contracted Voigt natation, e_{ijk} and d_{ijk} are simplified as the second-order tensors e_{il} and d_{ik}. Subscript i represents the x, y and z directions, being represented by the numbers 1, 2 and 3. And the subscripts l and k refer to the second-tensor xx, yy, zz, yz, zx and xy, which can be represented by the 1, 2, 3, 4, 5 and 6 numbers. The relationship between e_{il}, d_{ik} and the elastic stiffness tensor C_{kl} is [53, 54]

$$e_{il} = d_{ik}C_{kl}. \tag{1}$$

The 2D materials essentially contain a certain thickness and can be subjected with stress and strain. Particularly, the out-of-plane stress and strain of 2D materials play a key role in practical application scenarios such as nano-self-powered devices and robot bionic skin. Herein, the in-plane and out-of-plane stress and strain for 2D material are all considered for researching the complete piezoelectric stress and strain matrix for $M_4X_3Y_3$ monolayers. The other works also considered the out-of-plane stress and strain for 2D material [31, 53, 54]. For these $M_4X_3Y_3$ monolayers with the space group $Pmm2$, the matrix e_{il} and C_{kl} are expressed as

$$e_{il} = \begin{pmatrix} 0 & 0 & 0 & 0 & e_{15} & 0 \\ 0 & 0 & 0 & e_{24} & 0 & 0 \\ e_{31} & e_{32} & e_{33} & 0 & 0 & 0 \end{pmatrix}, \tag{2}$$

$$C_{kl} = \begin{pmatrix} C_{11} & C_{12} & C_{13} & 0 & 0 & 0 \\ C_{21} & C_{22} & C_{23} & 0 & 0 & 0 \\ C_{31} & C_{32} & C_{33} & 0 & 0 & 0 \\ 0 & 0 & 0 & C_{44} & 0 & 0 \\ 0 & 0 & 0 & 0 & C_{55} & 0 \\ 0 & 0 & 0 & 0 & 0 & C_{66} \end{pmatrix}, \tag{3}$$

from the formulas (1), (2) and (3), then the third-order piezoelectric strain d_{ik} tensor is expressed by

$$d_{ik} = \begin{pmatrix} 0 & 0 & 0 & 0 & d_{15} & 0 \\ 0 & 0 & 0 & d_{24} & 0 & 0 \\ d_{31} & d_{32} & d_{33} & 0 & 0 & 0 \end{pmatrix} \tag{4}$$

Therefore, according to Eqs. (1)–(4), the out-of-plane piezoelectric strain coefficients d_{31}, d_{32} and d_{33} are

Table 1 The out-of-plane piezoelectric stress e_{il} (pC/m) and strain d_{ik} (pm/V) coefficients for five fully relaxed $M_4X_3Y_3$ monolayers.

Structure	e_{31}	e_{32}	e_{33}	d_{31}	d_{32}	d_{33}
$Pd_4S_3Se_3$	37.42	27.97	30.22	0.50	0.46	3.92
$Pd_4S_3Te_3$	98.27	74.33	94.78	1.87	0.17	11.10
$Pd_4Se_3Te_3$	86.78	72.34	89.28	1.54	0.32	10.45
$Ni_4S_3Se_3$	77.20	61.41	64.99	0.92	0.17	2.53
$Ni_4Se_3Te_3$	551.54	577.20	533.26	7.93	5.81	61.57

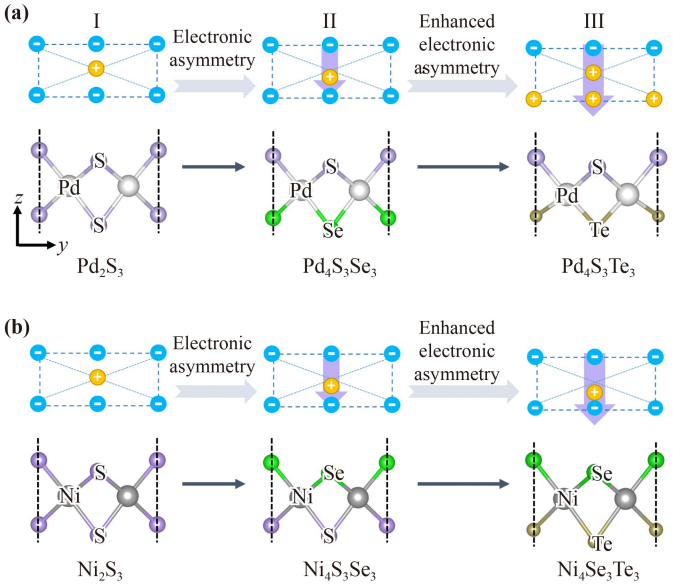

Fig. 5 **(a, b)** Schematic diagram of induced out-of-plane polarization in Pd_2S_3 and Ni_2S_3. The purple arrow indicates the polarization vector point toward the $-z$ axis direction.

expressed by [53]

$$d_{31} = \frac{Ae_{31} + Be_{32} + Ce_{33}}{G}, \tag{5}$$

$$d_{32} = \frac{De_{32} + Ee_{33} + Be_{31}}{G}, \tag{6}$$

$$d_{33} = \frac{Fe_{33} + Ce_{31} + Ee_{32}}{G}, \tag{7}$$

where $A = C_{22}C_{33} - C_{23}C_{23}$, $B = C_{23}C_{13} - C_{12}C_{33}$, $C = C_{12}C_{23} - C_{13}C_{22}$, $D = C_{33}C_{11} - C_{13}C_{13}$, $E = C_{13}C_{12} - C_{23}C_{11}$, $F = C_{22}C_{11} - C_{12}C_{12}$, $G = C_{22}(C_{11}C_{33} - C_{13}C_{13}) + C_{12}(C_{23}C_{13} - C_{12}C_{33}) + C_{23}(C_{13}C_{12} - C_{11}C_{23})$. Except the $Ni_4S_3Te_3$ without mechanical stability, values of piezoelectric stress e_{il} and strain d_{ik} coefficients for other five $M_4X_3Y_3$ monolayers are listed in Table 1.

Our results show that the strong piezoelectric materials can be obtained by the electron asymmetry through the intrinsically asymmetric atomic character of different chalcogen atoms. And it has also been confirmed that stronger piezoelectric materials can be obtained by further enhancing electronic asymmetry. As shown in Fig. 5(a), in Pd_2S_3 monolayer, when the top S bottom layer S atoms are replaced by Se atoms, the $Pd_4S_3Se_3$ monolayer is constructed, which contains the out-of-plane piezoelectricity. Importantly, the piezoelectricity is increased with the enhancing electron asymmetry, which increased by the introduction of Te atoms with smaller electronegativity of 2.1. Therefore, the $Pd_4S_3Te_3$ and $Pd_4Se_3Te_3$ monolayers possess stronger piezoelectricity than $Pd_4S_3Se_3$. As shown in Table 1, for $Pd_4X_3Y_3$ monolayers, their out-of-plane piezoelectric strain coefficients d_{31} (ranges from 0.5 to 1.54 pm/V), d_{32} (0.46 to 70.32 pm/V) and d_{33} (3.92 to 10.45 pm/V), which are comparable to and even larger than many reported 2D materials [22, 56–59]. It is worth mentioning that outmost $d_{33} = 11.10$ pm/V is found in $Pd_4S_3Te_3$ due to its strongest electron asymmetry among $Pd_4X_3Y_3$ monolayers. Moreover, the out-of-plane piezoelectricity is also introduced in $Ni_4S_3Se_3$ via replacing the top layer S atoms with Se atoms in Ni_2S_3 [Fig. 5(b)]. We further replace bottom layer S atoms with the Te atom to enhance electron asymmetry, thereby obtaining a strongest piezoelectric $Ni_4Se_3Te_3$ monolayer. Benefitting from the smallest $Y(\theta)$ and largest $v(\theta)$ among all $M_4X_3Y_3$ monolayers, the $Ni_4Se_3Te_3$ has the strongest out-of-plane piezoelectricity, with the $d_{31} = 7.93$ pm/V, $d_{32} = 5.81$ pm/V and $d_{33} = 61.57$ pm/V (Table 1). The out-of-plane piezoelectricity of $M_4X_3Y_3$ monolayers is much larger than that of many 2D materials (such as the oxygen functionalized MXenes (0.40–0.78 pm/V) [60], Janus TMDCs monolayers (0.03 pm/V) [30], Janus group-III materials (0.46 pm/V) [61] and In_2Se_3 (0.415 pm/V) [62]), and is comparable to that of MoSTe multilayers (5.7–13.5 pm/V) [30]. These strong out-of-plane polarization properties are originating from the uneven charge distribution due to electronegativity difference between X and Y atoms.

We then use the electronegativity difference (R_{ed}) to analyze piezoelectric changes of the five mechanically stable $M_4X_3Y_3$ monolayers. The ratio of electronegativity difference (R_{ed}) for $M_4X_3Y_3$ monolayers can be expressed as

$$R_{ed} = \frac{|X_{eln} - M_{eln}|}{|Y_{eln} - M_{eln}|}, \tag{8}$$

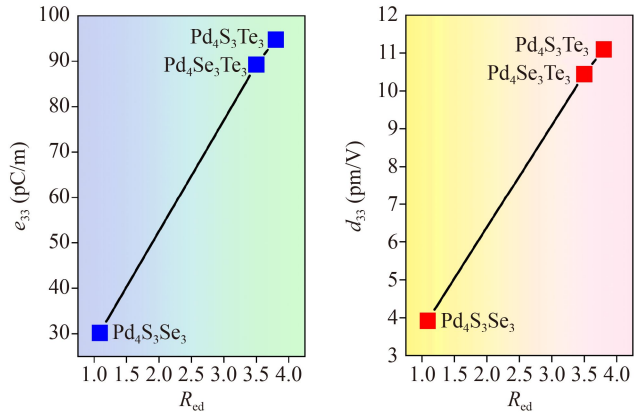

Fig. 6 The out-of-plane piezoelectric stress (e_{33}) and strain coefficients (d_{33}) as a function of the electronegativity difference ratio R_{ed} for $Pd_4X_3Y_3$ monolayers.

where X_{eln}, M_{eln}, and Y_{eln} represent the electronegativity of X (upper), Pd/Ni (middle) and Y (lower) atoms, respectively. The electronegativity of Pd, Ni, S, Se and Te atoms are 2.20, 1.91, 2.58, 2.55 and 2.10, respectively. Therefore, the calculated R_{ed} for $Pd_4S_3Se_3$, $Pd_4S_3Te_3$, $Pd_4Se_3Te_3$, $Ni_4S_3Se_3$ and $Ni_4Se_3Te_3$ monolayers is 1.09, 3.80, 3.50, 1.05 and 3.37, respectively. In Fig. 6 and Fig. S7 of the ESM, we find that the out-of-plane piezoelectric stress (e_{33}) and strain coefficients (d_{33}) increases with the increase of the differential charge density difference, which is consistent with previous studies, such as MoTO (T = S, Se or Te) monolayers [31], and the group-III(A) Janus hydrofluoride monolayers [53]. In other words, the intrinsically asymmetric atomic character of X and Y atoms can effectively regulate the piezoelectricity of $M_4X_3Y_3$ monolayers.

In $Pd_4X_3Y_3$ monolayers, the position of positive and negative charge centers along the z direction is remarked in Fig. 7(a). The vertical distance (characterized by l) between positive and negative charge centers and the total polarized charge value of centers (characterized by q) are both important factors affecting the electric dipole moment P ($P = ql$). $Pd_4S_3Se_3$, $Pd_4S_3Te_3$ and $Pd_4Se_3Te_3$ monolayers have $l_1 = 0.535$ Å, $l_2 = 2.093$ Å and $l_3 = 2.971$ Å, respectively. And the q for $Pd_4S_3Se_3$, $Pd_4S_3Te_3$ and $Pd_4Se_3Te_3$ monolayers is 0.947 e/cell, 0.700 e/cell and 0.345 e/cell, respectively. Therefore, $Pd_4S_3Se_3$ monolayer possesses the smallest electric dipole moment P of 0.507 eÅ/cell, corresponding to its smallest piezoelectric coefficients e_{33} and d_{33}. Compared to $Pd_4Se_3Te_3$ with the P of 1.025 eÅ/cell, the $Pd_4S_3Te_3$ contains the largest electric dipole moment P of 1.464 eÅ/cell and the largest e_{33} and d_{33}. Moreover, as shown in Fig. S7 of the ESM, the $Ni_4Se_3Te_3$ with P of 0.814 eÅ/cell has lager e_{33} and d_{33} than that of $Ni_4S_3Se_3$ monolayer with P of 0.379 eÅ/cell. Obviously, the out-of-plane piezoelectricity of $Pd_4X_3Y_3$ monolayers is positively correlated with the electric dipole moment P [Fig. 7(b)]. The interesting relationship between piezoelectricity and electronegativity difference ratio R_{ed}, as well as the interesting relationship with electric dipoles P, provides us with new ideas for the design of excellent piezoelectric nanomaterials. In short, the intrinsically asymmetric atomic character is important in regulating piezoelectricity of 2D materials. The ultra-high out-of-plane piezoelectricity makes $Pd_4X_3Y_3$ monolayers possessing significant potential applications in piezoelectric nano-devices, such as the collection of blue energy (wind, waves, etc.) and the conversion of tiny mechanical energy (human walking, body shaking, and hand touch).

4 Conclusions

In summary, we systematically investigated a family of 2D materials with strong out-of-plane piezoelectricity, namely $M_4X_3Y_3$ (X/Y = S, Se or Te, X ≠ Y) monolayers. Uneven charge distribution in favors of the generation of

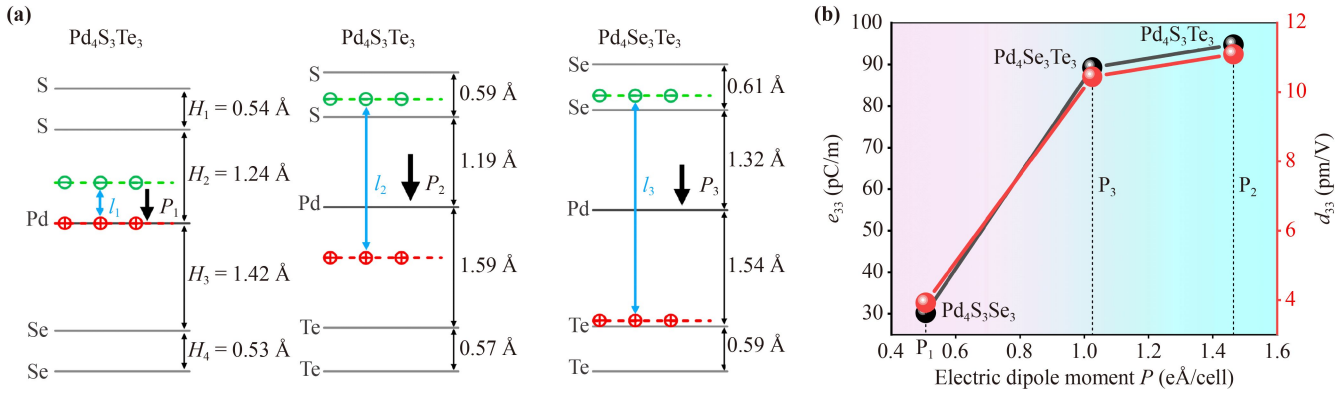

Fig. 7 **(a)** Position of the positive and negative charge centers in $Pd_4X_3Y_3$ along the z direction. Blue arrows are the vertical distance l between positive and negative charge centers; black arrows are the electric dipole moments P; H_1, H_2, H_3, and H_4 represent the vertical distances between two adjacent atomic layers, respectively. **(b)** The e_{33} and d_{33} as a function of the electric dipole moment P for $Pd_4X_3Y_3$ monolayers.

out-of-plane polarization. $Ni_4Se_3Te_3$ monolayer possesses the remarkable out-of-plane piezoelectricity with largest d_{33} of 61.57 pm/V, which is much larger than that of most known 2D materials. Importantly, we proposed an achieving strategy for introducing strong piezoelectricity in 2D materials via the electronic asymmetry induced by the intrinsically asymmetric atomic character of different chalcogen atoms. And this strategy has been validated in $M_4X_3Y_3$ materials, proving that the piezoelectricity is greatly regulated by enhancing the electronic asymmetry. Electronegativity difference ratio R_{ed} and electric dipole moment P effectively predict the strength of out-of-plane piezoelectricity for 2D materials because piezoelectric coefficients are related with the R_{ed} and P. These $M_4X_3Y_3$ nanomaterials with strong out-of-plane piezoelectricity can serve as alternative materials for energy-harvesting nanodevices or self-powered wearables. Our work offers useful design guidelines for the discovery of 2D strong piezoelectric materials.

Declaration of competing interest The authors declare that they have no known competing financial interests or personal relationships that could have appeared to influence the work reported in this paper.

Electronic supplementary materials The online version contains supplementary material available at https://doi.org/10.1007/s11467-023-1348-5 and https://journal.hep.com.cn/fop/EN/10.1007/s11467-023-1348-5.

Acknowledgements This work was supported by the National Natural Science Foundation of China (Grant No. 11474123).

References

1. K. S. Novoselov, A. K. Geim, S. V. Morozov, D. Jiang, Y. Zhang, S. V. Dubonos, I. V. Grigorieva, and A. A. Firsov, Electric field effect in atomically thin carbon films, *Science* 306(5696), 666 (2004)
2. C. Yang, Y. Wu, Y. Wang, H. N. Zhang, L. H. Zhu, and X. C. Wang, Electronic properties of double-atom catalysts for electrocatalytic oxygen evolution reaction in alkaline solution: A DFT study, *Nanoscale* 14(1), 187 (2021)
3. L. L. Liu, C. P. Chen, L. S. Zhao, Y. Wang, and X. C. Wang, Metal-embedded nitrogen-doped graphene for H_2O molecule dissociation, *Carbon* 115, 773 (2017)
4. R. Guo, Y. Guo, Y. Zhang, X. Gong, T. Zhang, X. Yu, S. Yuan, and J. Wang, Electron doping induced stable ferromagnetism in two-dimensional GdI_3 monolayer, *Front. Phys.* 18(4), 43304 (2023)
5. S. Li, W. Ji, J. Zhang, Y. Wang, C. Zhang, and S. Yan, Two-dimensional rectangular bismuth bilayer: A novel dual topological insulator, *Front. Phys.* 18(4), 43301 (2023)
6. G. Zheng, S. Qu, W. Zhou, and F. Ouyang, Janus monolayer TaNF: A new ferrovalley material with large valley splitting and tunable magnetic properties, *Front. Phys.* 18(5), 53302 (2023)
7. D. Çakır, F. M. Peeters, and C. Sevik, Mechanical and thermal properties of h-MX_2 (M = Cr, Mo, W; X = O, S, Se, Te) monolayers: A comparative study, *Appl. Phys. Lett.* 104(20), 203110 (2014)
8. Y. Mogulkoc, R. Caglayan, and Y. O. Ciftci, Band alignment in monolayer boron phosphide with Janus MoSSe heterobilayers under strain and electric field, *Phys. Rev. Appl.* 16(2), 024001 (2021)
9. S. D. Guo, X. S. Guo, Y. T. Zhu, and Y. S. Ang, Predicted ferromagnetic monolayer CrSCl with large vertical piezoelectric response: A first-principles study, *Appl. Phys. Lett.* 121(6), 062403 (2022)
10. S. D. Guo, J. X. Zhu, W. Q. Mu, and B. G. Liu, Possible way to achieve anomalous valley Hall effect by piezoelectric effect in a $GdCl_2$ monolayer, *Phys. Rev. B* 104(22), 224428 (2021)
11. S. D. Guo, Y. L. Tao, W. Q. Mu, and B. G. Liu, Correlation-driven threefold topological phase transition in monolayer $OsBr_2$, *Front. Phys.* 18(3), 33304 (2023)
12. A. Chandrasekaran, A. Mishra, and A. K. Singh, Ferroelectricity, antiferroelectricity, and ultrathin 2D electron/hole gas in multifunctional monolayer MXene, *Nano Lett.* 17(5), 3290 (2017)
13. Z. Jiang, P. Wang, X. Jiang, and J. Zhao, MBene (MnB): A new type of 2D metallic ferromagnet with high Curie temperature, *Nanoscale Horiz.* 3(3), 335 (2018)
14. B. Zhang, J. Zhou, and Z. Sun, MBenes: Progress, challenges and future, *J. Mater. Chem. A* 10(30), 15865 (2022)
15. Y. L. Hong, Z. Liu, L. Wang, T. Zhou, W. Ma, C. Xu, S. Feng, L. Chen, M. L. Chen, D. M. Sun, X. Q. Chen, H. M. Cheng, and W. Ren, Chemical vapor deposition of layered two-dimensional $MoSi_2N_4$ materials, *Science* 369(6504), 670 (2020)
16. S. D. Guo, Y. L. Tao, H. T. Guo, Z. Y. Zhao, B. Wang, G. Wang, and X. Wang, Possible electronic state quasi-half-valley metal in a VGe_2P_4 monolayer, *Phys. Rev. B* 107(5), 054414 (2023)
17. S. D. Guo, W. Q. Mu, J. H. Wang, Y. X. Yang, B. Wang, and Y. S. Ang, Strain effects on the topological and valley properties of the Janus monolayer $VSiGeN_4$, *Phys. Rev. B* 106(6), 064416 (2022)
18. Y. Wu, Y. Ma, H. Zheng, and S. Ramakrishna, Piezoelectric materials for flexible and wearable electronics: A review, *Mater. Des.* 211, 110164 (2021)
19. C. Zhang, W. Yuan, B. Zhang, O. Yang, Y. Liu, L. He, J. Wang, and Z. L. Wang, High space efficiency hybrid nanogenerators for effective water wave energy harvesting, *Adv. Funct. Mater.* 32(18), 2111775 (2022)
20. Y. Jiang, J. An, F. Liang, G. Zuo, J. Yi, C. Ning, H. Zhang, K. Dong, and Z. L. Wang, Knitted self-powered sensing textiles for machine learning-assisted sitting posture monitoring and correction, *Nano Res.* 15(9), 8389 (2022)
21. R. Cheng, C. Ning, P. Chen, F. Sheng, C. Wei, Y. Zhang, X. Peng, K. Dong, and Z. L. Wang, Enhanced output of on-body direct-current power textiles by efficient energy management for sustainable working of mobile electronics, *Adv. Energy Mater.* 12(29), 2201532 (2022)

22. Y. Wu, C. H. Yang, H. N. Zhang, L. H. Zhu, X. Y. Wang, Y. Q. Li, S. Y. Zhu, and X. C. Wang, The flexible Janus X_2PAs (X = Si, Ge and Sn) monolayers with in-plane and out-of-plane piezoelectricity, *Appl. Surf. Sci.* 589, 152999 (2022)
23. Y. Q. Li, X. Y. Wang, S. Y. Zhu, D. S. Tang, Q. W. He, and X. C. Wang, Enhanced vertical polarization and ultra-low polarization switching barriers of two-dimensional SnS/SnSSe ferroelectric heterostructures, *J. Mater. Chem. C* 10(33), 12132 (2022)
24. H. R. Gutiérrez, N. Perea-López, A. L. Elías, A. Berkdemir, B. Wang, R. Lv, F. López-Urías, V. H. Crespi, H. Terrones, and M. Terrones, Extraordinary room-temperature photoluminescence in triangular WS_2 monolayers, *Nano Lett.* 13(8), 3447 (2013)
25. J. Qi, Y. W. Lan, A. Z. Stieg, J. H. Chen, Y. L. Zhong, L. J. Li, C. D. Chen, Y. Zhang, and K. L. Wang, Piezoelectric effect in chemical vapour deposition-grown atomic-monolayer triangular molybdenum disulfide piezotronics, *Nat. Commun.* 6(1), 7430 (2015)
26. W. Wu, L. Wang, Y. Li, F. Zhang, L. Lin, S. Niu, D. Chenet, X. Zhang, Y. Hao, T. F. Heinz, J. Hone, and Z. L. Wang, Piezoelectricity of single-atomic-layer MoS_2 for energy conversion and piezotronics, *Nature* 514(7523), 470 (2014)
27. J. H. Lee, J. Y. Park, E. B. Cho, T. Y. Kim, S. A. Han, T. H. Kim, Y. Liu, S. K. Kim, C. J. Roh, H. J. Yoon, H. Ryu, W. Seung, J. S. Lee, J. Lee, and S. W. Kim, Reliable piezoelectricity in bilayer WSe_2 for piezoelectric nanogenerators, *Adv. Mater.* 29(29), 1606667 (2017)
28. E. Nasr Esfahani, T. Li, B. Huang, X. Xu, and J. Li, Piezoelectricity of atomically thin WSe_2 via laterally excited scanning probe microscopy, *Nano Energy* 52, 117 (2018)
29. C. Zhang, Y. Nie, S. Sanvito, and A. Du, First-principles prediction of a room-temperature ferromagnetic Janus VSSe monolayer with piezoelectricity, ferroelasticity, and large valley polarization, *Nano Lett.* 19(2), 1366 (2019)
30. L. Dong, J. Lou, and V. B. Shenoy, Large in-plane and vertical piezoelectricity in janus transition metal dichalchogenides, *ACS Nano* 11(8), 8242 (2017)
31. Y. Q. Li, X. Y. Wang, S. Y. Zhu, D. S. Tang, Q. W. He, and X. C. Wang, Active asymmetric electron-transfer effect on the enhanced piezoelectricity in MoTO (T = S, Se, or Te) monolayers and bilayers, *J. Phys. Chem. Lett.* 13(41), 9654 (2022)
32. S. S. Naghavi, J. He, and C. Wolverton, Crystal and electronic structures of palladium sesquichalcogenides, *Chem. Mater.* 33(7), 2298 (2021)
33. S. S. Naghavi, J. He, Y. Xia, and C. Wolverton, Pd_2Se_3 monolayer: A promising two-dimensional thermoelectric material with ultralow lattice thermal conductivity and high power factor, *Chem. Mater.* 30(16), 5639 (2018)
34. J. Lin, S. Zuluaga, P. Yu, Z. Liu, S. T. Pantelides, and K. Suenaga, Novel Pd_2Se_3 two-dimensional phase driven by interlayer fusion in layered $PdSe_2$, *Phys. Rev. Lett.* 119(1), 016101 (2017)
35. Z. Moradi, M. Vaezzadeh, and M. Saeidi, Thermoelectric, spin-dependent optical and quantum transport properties of 2D half-metallic Co_2Se_3, *Phys. Chem. Chem. Phys.* 24(36), 22016 (2022)
36. P. Lv, G. Tang, C. Yang, J. Deng, Y. Liu, X. Wang, X. Wang, and J. Hong, Half-metallicity in two-dimensional Co_2Se_3 monolayer with superior mechanical flexibility, *2D Mater.* 5(4), 045026 (2018)
37. Y. Luo, M. Sun, J. Yu, and U. Schwingenschlögl, $Pd_4S_3Se_3$, $Pd_4S_3Te_3$, and $Pd_4Se_3Te_3$: Candidate two-dimensional Janus materials for photocatalytic water splitting, *Chem. Mater.* 33(11), 4128 (2021)
38. G. Kresse and J. Hafner, *Ab initio* molecular dynamics for liquid metals, *Phys. Rev. B* 47(1), 558 (1993)
39. G. Kresse and J. Hafner, Ab initio molecular-dynamics simulation of the liquid-metal-amorphous-semiconductor transition in germanium, *Phys. Rev. B* 49(20), 14251 (1994)
40. J. P. Perdew, K. Burke, and M. Ernzerhof, Generalized gradient approximation made simple, *Phys. Rev. Lett.* 77(18), 3865 (1996)
41. D. Alfè, PHON: A program to calculate phonons using the small displacement method, *Comput. Phys. Commun.* 180(12), 2622 (2009)
42. S. Nosé, A unified formulation of the constant temperature molecular dynamics methods, *J. Chem. Phys.* 81(1), 511 (1984)
43. J. Heyd and G. E. Scuseria, Assessment and validation of a screened Coulomb hybrid density functional, *J. Chem. Phys.* 120(16), 7274 (2004)
44. G. Henkelman, A. Arnaldsson, and H. Jónsson, A fast and robust algorithm for Bader decomposition of charge density, *Comput. Mater. Sci.* 36(3), 354 (2006)
45. X. Wu, D. Vanderbilt, and D. R. Hamann, Systematic treatment of displacements, strains, and electric fields in density-functional perturbation theory, *Phys. Rev. B* 72(3), 035105 (2005)
46. C. Tang, L. Zhang, S. Sanvito, and A. Du, Enabling room-temperature triferroic coupling in dual transition-metal dichalcogenide monolayers via electronic asymmetry, *J. Am. Chem. Soc.* 145(4), 2485 (2023)
47. J. Chen, G. H. Ryu, S. Sinha, and J. H. Warner, Atomic structure and dynamics of defects and grain boundaries in 2D Pd_2Se_3 monolayers, *ACS Nano* 13(7), 8256 (2019)
48. I. Eren and B. Akgenc, Tuning the structural, electronic and dynamical properties of Janus $M_4X_3Y_3$ (M = Pd, Ni and Co; X, Y = S, Se and Te) monolayers: A DFT study, *Phys. Chem. Chem. Phys.* 23(37), 21139 (2021)
49. W. Xiong, K. Huang, and S. Yuan, The mechanical, electronic and optical properties of two-dimensional transition metal chalcogenides MX_2 and M_2X_3 (M = Ni, Pd; X = S, Se, Te) with hexagonal and orthorhombic structures, *J. Mater. Chem. C* 7(43), 13518 (2019)
50. J. Zhao, Y. Zhao, H. He, P. Zhou, Y. Liang, and T. Frauenheim, Stacking engineering: A boosting strategy for 2D photocatalysts, *J. Phys. Chem. Lett.* 12(41), 10190 (2021)
51. R. Peng, Y. Ma, B. Huang, and Y. Dai, Two-dimensional Janus PtSSe for photocatalytic water splitting under the visible or infrared light, *J. Mater. Chem. A* 7(2), 603 (2019)
52. Y. Yu, J. Zhou, Z. Guo, and Z. Sun, Novel two-dimensional Janus $MoSiGeN_4$ and $WSiGeN_4$ as highly efficient

photocatalysts for spontaneous overall water splitting, *ACS Appl. Mater. Interfaces* 13(24), 28090 (2021)

53. H. N. Zhang, Y. Wu, C. Yang, L. H. Zhu, and X. C. Wang, Enhanced out-of-plane piezoelectricity of group-III(A) Janus hydrofluoride monolayers, *Phys. Rev. B* 104(23), 235437 (2021)
54. H. N. Zhang, C. Yang, Y. Q. Li, S. Y. Zhu, X. Y. Wang, Q. W. He, D. S. Tang, and X. C. Wang, Large out-of-plane piezoelectricity of VIA group functionalized MXenes thin films for MEMS, *Appl. Phys. Lett.* 121(14), 143504 (2022)
55. M. Yagmurcukardes, R. T. Senger, F. M. Peeters, and H. Sahin, Mechanical properties of monolayer GaS and GaSe crystals, *Phys. Rev. B* 94(24), 245407 (2016)
56. M. Yagmurcukardes and F. M. Peeters, Stable single layer of Janus MoSO: Strong out-of-plane piezoelectricity, *Phys. Rev. B* 101(15), 155205 (2020)
57. S. D. Guo, Y. T. Zhu, K. Qin, and Y. S. Ang, Large out-of-plane piezoelectric response in ferromagnetic monolayer NiClI, *Appl. Phys. Lett.* 120(23), 232403 (2022)
58. Y. F. Zhao, Y. H. Shen, H. Hu, W. Y. Tong, and C. G. Duan, Combined piezoelectricity and ferrovalley properties in Janus monolayer VClBr, *Phys. Rev. B* 103(11), 115124 (2021)
59. Y. Q. Li, H. N. Zhang, C. Yang, X. Y. Wang, S. Y. Zhu, and X. C. Wang, Ferroelastic Zr_2P_2XY (X/Y = I, Br, Cl or F; X ≠ Y) monolayers with tunable in-plane electronic anisotropy and remarkable out-of-plane piezoelectricity, *Appl. Surf. Sci.* 608, 155202 (2023)
60. J. Tan, Y. Wang, Z. Wang, X. He, Y. Liu, B. Wang, M. I. Katsnelson, and S. Yuan, Large out-of-plane piezoelectricity of oxygen functionalized MXenes for ultrathin piezoelectric cantilevers and diaphragms, *Nano Energy* 65, 104058 (2019)
61. Y. Guo, S. Zhou, Y. Bai, and J. Zhao, Enhanced piezoelectric effect in Janus group-III chalcogenide monolayers, *Appl. Phys. Lett.* 110(16), 163102 (2017)
62. L. Hu and X. Huang, Peculiar electronic, strong in-plane and out-of-plane second harmonic generation and piezoelectric properties of atom-thick α-M_2X_3 (M = Ga, In; X = S, Se): Role of spontaneous electric dipole orientations, *RSC Adv.* 7(87), 55034 (2017)